AGU PUBLICATIONS

Geophysical Research Letters

RESEARCH LETTER
10.1002/2015GL063731

Key Points:
- Cyclonic vorticity is generated in the sloped turbulent bottom boundary layer
- The flow separates and becomes unstable to horizontal shear instability
- The flow rolls up and forms a street of submesoscale cyclonic vortices

Correspondence to:
J. Gula,
gula@atmos.ucla.edu

Citation:
Gula, J., M. J. Molemaker, and J. C. McWilliams (2015), Topographic vorticity generation, submesoscale instability, and vortex street formation in the Gulf Stream, *Geophys. Res. Lett.*, *42*, 4054–4062, doi:10.1002/2015GL063731.

Received 13 MAR 2015
Accepted 25 APR 2015
Accepted article online 2 MAY 2015
Published online 23 MAY 2015

Topographic vorticity generation, submesoscale instability and vortex street formation in the Gulf Stream

J. Gula[1], M. J. Molemaker[1], and J. C. McWilliams[1]

[1]Department of Atmospheric and Oceanic Sciences, University of California, Los Angeles, California, USA

Abstract Meanders and eddies are routinely observed in the Gulf Stream along the South Atlantic Bight. We analyze here the instability processes that lead to the formation of submesoscale eddies on the cyclonic side of the Gulf Stream at the exit of the Florida Straits using very high resolution realistic simulations. The positive relative vorticity and potential vorticity on the cyclonic side of the Gulf Stream are strongly intensified in the Straits due to topographic drag along the continental slope. The bottom drag amplifies the cyclonic shear by generating large positive vertical vorticity values within the sloped turbulent bottom boundary layer. Downstream from the Straits the current becomes unstable to horizontal shear instability, rolls up, and forms a street of submesoscale vortices. The vortices expand as they propagate northward along the shelf, where they can generate large vertical displacements and enhance cross-shelf exchanges.

1. Introduction

There is an intense eddy generation in the Gulf Stream along the South Atlantic Bight (SAB). Satellite observations show a steady increase in the eddy activity between the Florida Straits and the Charleston Bump at 31°N, followed by a sharp increase downstream of the Bump and a gradual decay from approximately 33°N to Cape Hatteras [*Olson et al.*, 1983]. The Charleston Bump is a well known and preferred location for the generation of mesoscale frontal eddies [*Gula et al.*, 2015]. In the region between the Florida Straits and the Charleston Bump, there are also a large number of eddies, usually smaller in size, as seen in satellite observations (Figure 1). Signatures of the eddies are seen at the surface in the form of negative temperature anomalies and warm streamers of water ("shingles") extending over the shelf [*von Arx et al.*, 1955]. The eddies contribute to shelf water mass and heat exchange and play a role in the energy balance of the Gulf Stream [*Lee et al.*, 1991; *Gula et al.*, 2015].

We present in the following results from realistic simulations of the Gulf Stream region realized with the Regional Oceanic Modeling System (ROMS) [*Shchepetkin and McWilliams*, 2005]. The use of a sigma coordinate, with significant grid stretching near the bottom so that the boundary layer profile is reasonably well resolved, is of great advantage in calculating flows over complex terrain. We use a nesting approach with successive horizontal grid nesting refinements from a parent grid resolution of $\Delta x \approx 6$ km covering most of the Atlantic Ocean to successive child grids with $\Delta x \approx 2.5$ km and $\Delta x \approx 750$ m. The procedure is described in detail in *Gula et al.* [2015], where characteristics of the mean structure and variability of the Gulf Stream in the simulation have been validated against satellite and in situ observations. All the results presented in the following come from the finer-resolution nest.

The sources of the eddy kinetic energy (EKE) along the SAB are quantified following *Gula et al.* [2015]. The eddy kinetic energy is written as $\mathrm{EKE} = 0.5(\langle u'^2 \rangle + \langle v'^2 \rangle)$, where (u, v) are the horizontal velocities in the cross- and along-front directions (x, y), positive in the offshore and downstream directions, respectively. The brackets denote a time average, and the prime denotes fluctuations relative to the time average. Along-stream variations of EKE in the Gulf Stream are reproduced for the SAB sector between 26°N and 31°N in Figure 2. The conversion from mean to eddy kinetic energy due to the horizontal shear is $\mathrm{HRS} = -\langle \mathbf{u}'v' \rangle \frac{\partial \langle \mathbf{u} \rangle}{\partial y} - \langle \mathbf{u}'u' \rangle \frac{\partial \langle \mathbf{u} \rangle}{\partial x}$. The conversion from eddy potential to eddy kinetic energy corresponds to the vertical buoyancy flux $\mathrm{VBF} = \langle w'b' \rangle$, where w is the vertical velocity and b the buoyancy anomaly. Predominance of one of these two source terms indicates that the eddy generation mechanism is primarily a baroclinic instability (VBF > 0) or a barotropic instability (HRS > 0). The conversion from mean to eddy kinetic energy due to the vertical shear is small and does not significantly impact the flow (not shown). The variations of EKE along the Stream show a

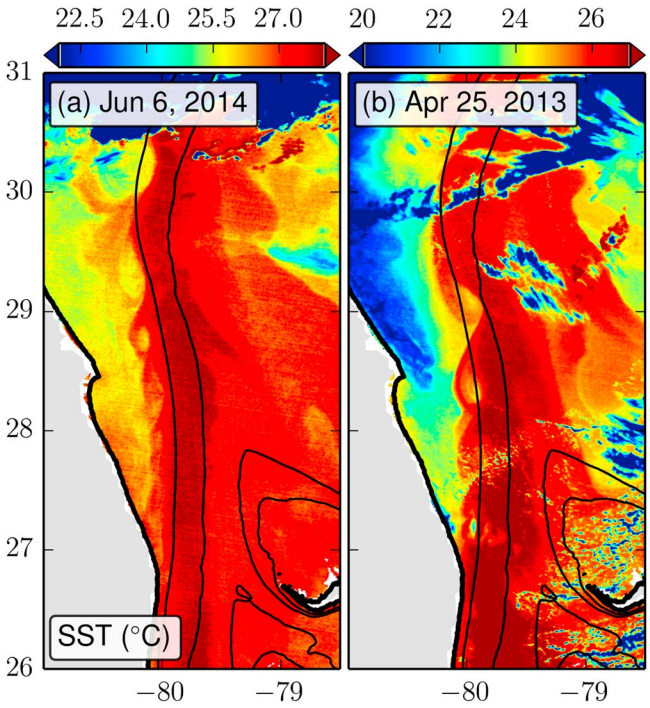

Figure 1. Observed sea surface temperature (SST) of the Gulf Stream along the Florida coast on (left) 6 June 2014 and (right) 25 April 2013. Bahamas contours are visible southeast of the domain. Data from Moderate Resolution Imaging Spectroradiometer (MODIS)-AQUA. Notice the Gulf Stream edge fluctuations on the shoreward side. Topography is shown in black contours by the 0 m, 200 m, and 600 m isobaths.

growth of eddy energy downstream of the Straits driven mostly by the contribution from the barotropic conversion HRS that is positive between 27°N and 30°N, and a small decrease of eddy energy between 30°N and the Charleston Bump at 31°N (Figure 2). The baroclinic energy conversion is always positive but has a smaller amplitude than the barotropic one upstream of the Bump. This shows that the eddy activity between the Straits and the Bump is driven mostly by a barotropic conversion of kinetic energy from the mean flow to the eddies.

We argue that the main instability process downstream of the Florida Straits is a cyclonic analog of the mechanisms presented in *Molemaker et al.* [2015]. There is cyclonic vorticity generation by bottom drag when the Gulf Stream is flowing along the Florida slope, partial wake separation downstream of the Straits, and horizontal shear instability leading to submesoscale coherent vortex generation. A typical instability event in this region is shown in Figure 3 with a sequence of sea surface temperature (SST) and surface relative vorticity.

2. Bottom Vorticity Generation

The flow in the Florida Straits is strongly squeezed against topography on both sides. We focus here on the cyclonic side where the mean flow displays large positive relative vorticity values along the Florida slope. Along-stream variations of the relative vorticity maximum at $z = -50$ m are shown in Figure 2. The mean relative vorticity maximum increases strongly between 26°N and 27°N, where it reaches values up to $3-4f$ and slowly decreases between 27°N and 30°N. The peak value is reached immediately upstream of the starting point of the SAB, where the shelf starts to widen and the Gulf Stream loses contact with the upper shelf.

The bottom drag against the slope amplifies the cyclonic shear by generating large positive vertical vorticity values within the sloped turbulent bottom boundary layer, along the lines of the mechanism described in *Molemaker et al.* [2015]. The flow interacts with the topography through a vertical bottom boundary condition related to turbulent bottom stress, which exerts a drag on the lowest layers. But if this vertical boundary layer is over a sloping boundary, then the necessary vertical shear also implies a horizontal shear. Typical cross-stream vertical sections of instantaneous relative vorticity show the intensification of the horizontal velocity shear

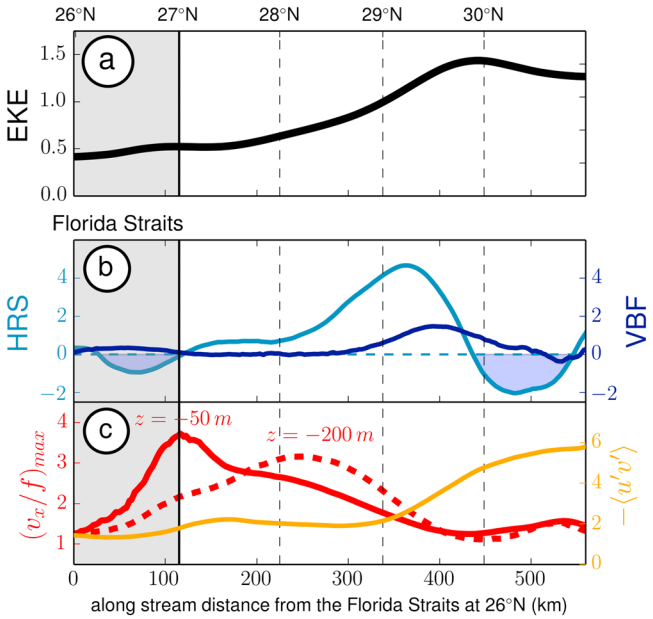

Figure 2. Annual mean along-stream (a) eddy kinetic energy EKE (black) and (b) barotropic energy conversion term HRS (blue) and baroclinic energy conversion term VBF (dark blue). These quantities have been integrated vertically over the entire water column and in the cross-stream direction over the full Stream and multiplied by the mean density $\rho_0 = 1027.4$ kg m^{-3} such that the unit of EKE is kg m s^{-1} = J m^{-1}, and the unit of the eddy conversion terms is J m^{-1} s^{-1}. (c) Maximum cross-stream gradient of along-stream surface velocity v_x/f at $z = -50$ m (solid red) and $z = -200$ m (dashed red), and surface eddy momentum flux $-\langle u'v' \rangle$ (yellow, in m^2 s^{-2}).

and relative vorticity along the Florida Coast in Figures 4a and 4b. The variations are consistent with the mean values in Figure 2, in particular the vorticity maximum at 26.8°N (Figure 4b), just before the Stream starts to lose contact with the shelf in the upper 50 m.

The vertical and horizontal scales of the boundary layer are locally about 50 m and 500 m with a cross-shelf bottom slope as high as 0.1 along the Florida Coast. Given a current of 0.5–1 m s^{-1}, we can evaluate the scale of the vertical vorticity in the boundary layer as $\mathcal{O}(10f - 20f)$, which is consistent with the instantaneous maximum values observed at the location of Figure 4b. The model has 50 levels in the vertical with grid stretching near the bottom such that the vertical resolution does not exceed 2 m in the region of strong topographic vorticity generation, between the surface and $z = -100$ m.

The sloped turbulent bottom boundary layer also provides a source of potential vorticity (PV). As first suggested by *Rhines* [1998] and later demonstrated by *Hallberg and Rhines* [2000] and *Williams and Roussenov* [2003], frictional stresses and diabatic mixing along a slope generate boundary PV, which can be stripped off by the current and injected in the ocean interior. PV is defined as $q = \boldsymbol{\omega}_\mathbf{a} \cdot \boldsymbol{\nabla} b$, the dot product of the absolute vorticity $\boldsymbol{\omega}_\mathbf{a} = f\mathbf{z} + \boldsymbol{\nabla} \times \mathbf{u}$ and the gradient of buoyancy $b = -g\frac{\rho}{\rho_0}$, where f is the Coriolis parameter, $\mathbf{z}$ the unit vertical vector, ρ the in situ density, ρ_0 the mean reference density, and g the gravitational acceleration. The mean PV of the flow increases along the Florida slope and reaches large positive values at the exit of the Florida Straits (Figures 4e and 4g). The flux form of the PV equation is

$$\frac{\partial q}{\partial t} + \boldsymbol{\nabla}.[\underbrace{q\mathbf{u}}_{\text{adv.}} - \underbrace{\boldsymbol{\omega}_\mathbf{a} \cdot \frac{Db}{Dt}}_{\text{diab.}} + \underbrace{\boldsymbol{\nabla} b \times \mathbf{F}}_{\text{non conser.}}] = 0, \tag{1}$$

where $\mathbf{F}$ are the non conservative forces per unit mass [*Marshall et al.*, 2001]. The injection of PV at the bottom can be computed as $\mathbf{J}_{\text{bot}} \cdot \mathbf{n} = \boldsymbol{\nabla} b \times \mathbf{F}_b \cdot \mathbf{n}$, where $\mathbf{n}$ is the unit vector normal to the bottom pointing into the ocean and $\mathbf{F}_b$ is the vertical gradient of stress at the bottom. By integrating over the boundary layer depth, it can be approximated as $\mathbf{F}_b \approx -\frac{C_d|\mathbf{u}_b|}{\rho_0 h_{bbl}}\mathbf{u}_b$, where $\mathbf{u}_b$ is the velocity at the bottom, C_d is the quadratic bulk drag coefficient using a Von Karman log layer, and h_{bbl} is the depth of the bottom boundary layer. The mean bottom flux of PV, $\mathbf{J}_{\text{bot}}$, reaches amplitudes up to 10^{-9} m s^{-4} over the Florida slope (Figure 4f), which are several orders of magnitude larger than the local values of the mean surface fluxes of PV due to wind and buoyancy forcing

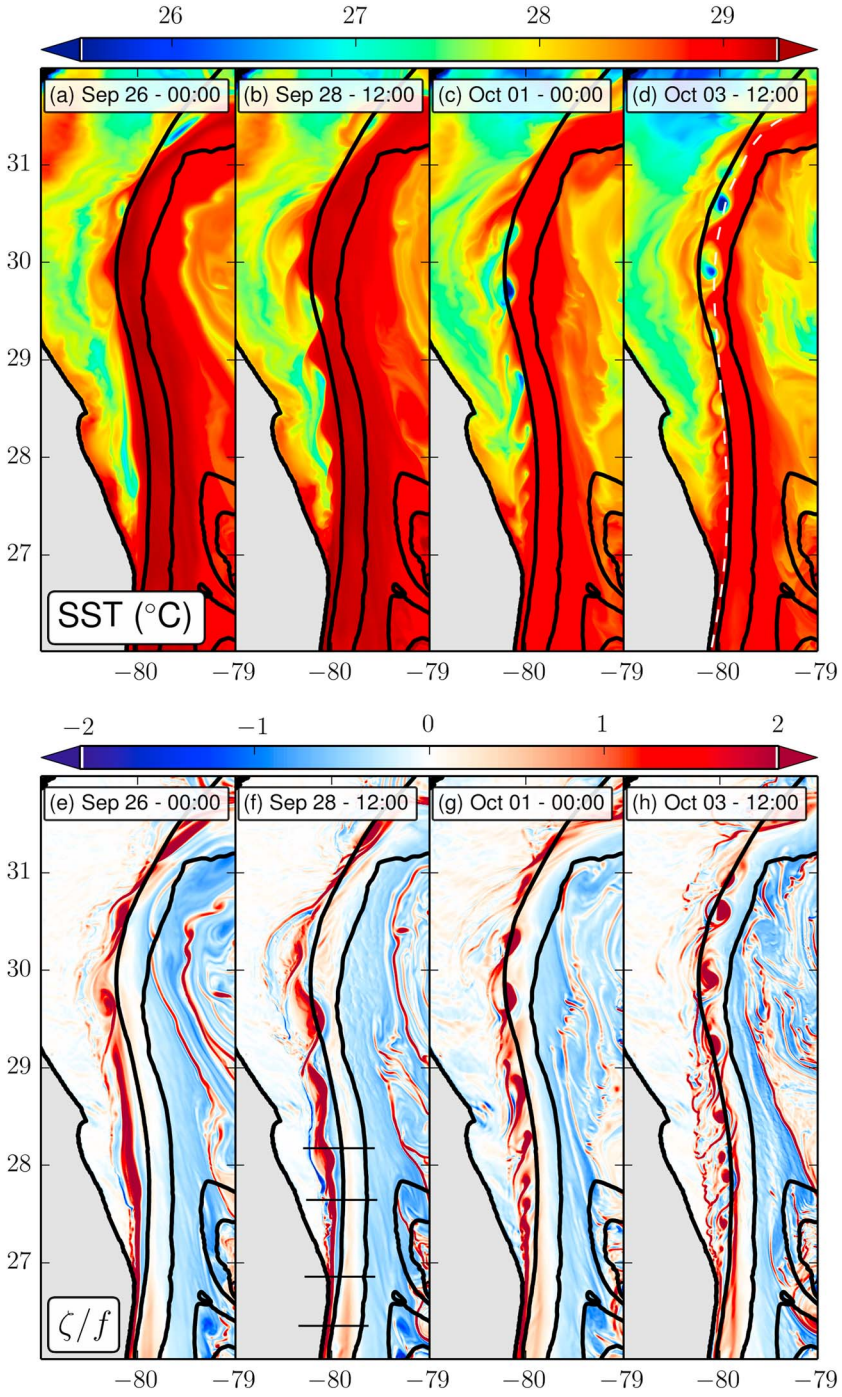

Figure 3. Snapshots of SST (top) and surface relative vorticity normalized by f (bottom). Barotropic instability of the flow is visible between the Florida Straits and the Charleston Bump in the form of a cyclonic vortex street. Time interval between two panels is 2.5 days. Topography is shown in black contours at 0 m, 200 m, and 600 m isobaths. The straight black lines perpendicular to the streamflow in Figure 3f show the locations of the vertical sections plotted in Figure 4. The dashed white line in Figure 3d shows the location of the vertical sections plotted in Figure 6.

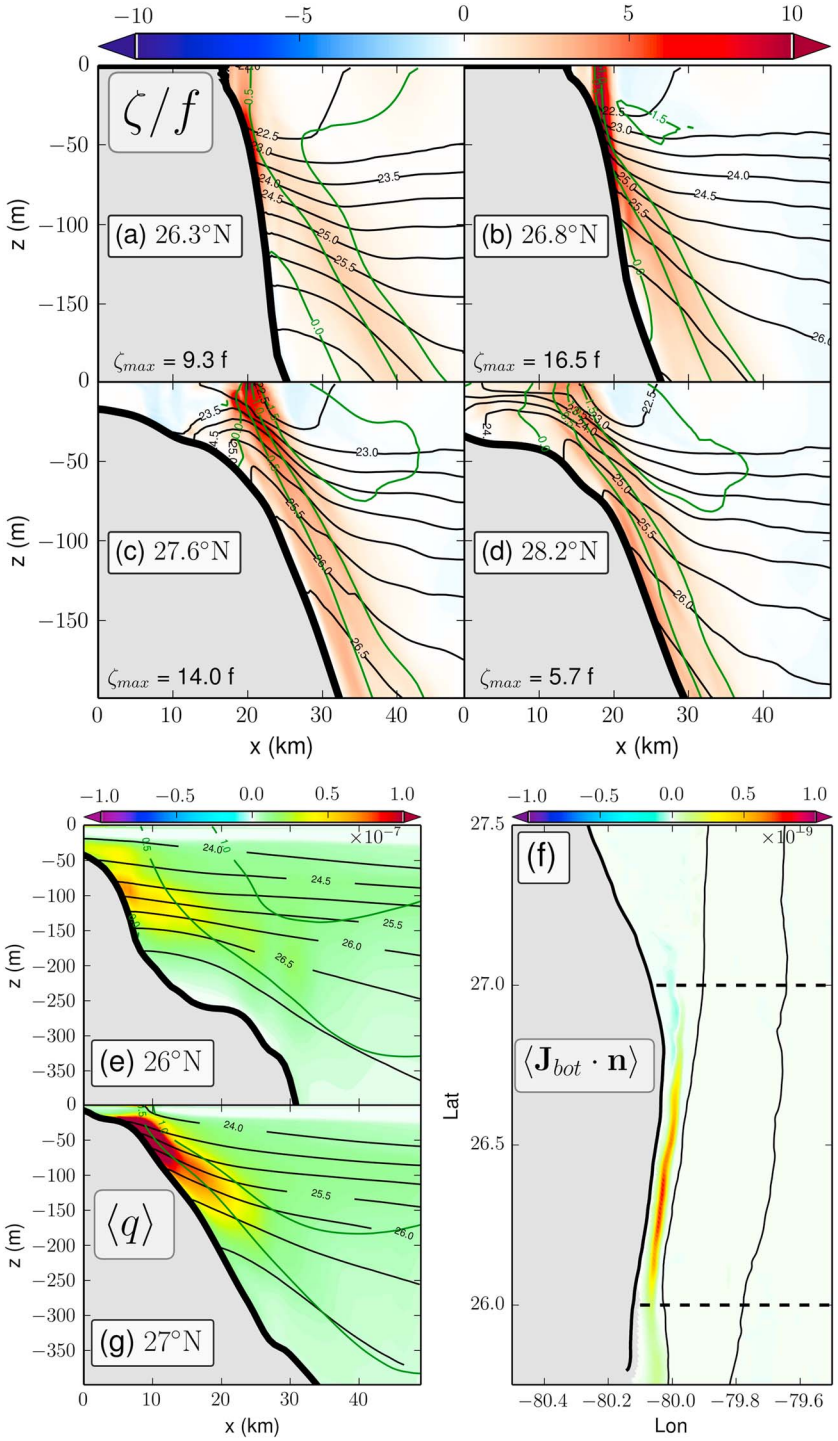

Figure 4. (a–d) Instantaneous relative vorticity normalized by f (colors), density (black contours, in kg m^{-3}) and along-stream velocity (green contours, in m s^{-1}) along the vertical cross-shelf sections marked as black lines in Figure 3f. Panels are plotted from upstream to downstream. Maximum relative vorticity values for each section are (a) 9.3f, (b) 16.5f, (c) 9.4f, and (d) 5.7f, consistent with drag generation of vorticity followed by vorticity mixing by the instability and vortex formation. (e, g) Time mean PV $\langle q \rangle$ (colors, in 10^{-7} s^{-3}), density (black contours), and along-stream velocity (green contours) at 26°N (e) and 27°N (g). (f) Time mean PV flux at the bottom $\langle \mathbf{J}_{bot} \cdot \mathbf{n} \rangle$ (in 10^{-9} m s^{-4}). Topography is shown in black contours by the 0 m, 200 m, and 600 m isobaths.

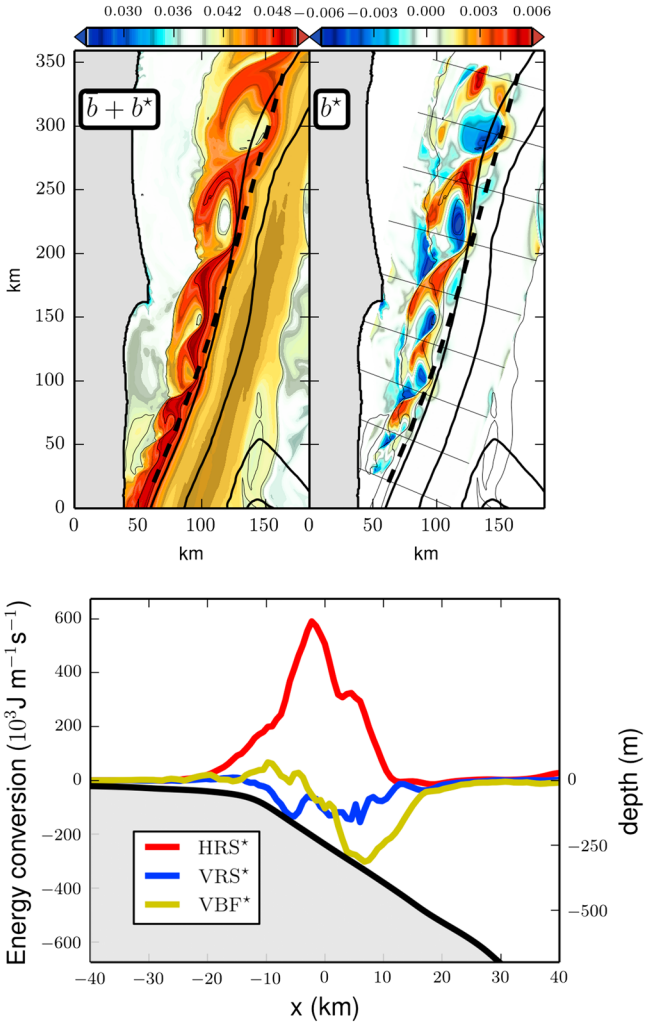

Figure 5. (top left) Total surface buoyancy field b with a black dashed line marking the along-stream axis and (top right) perturbation field $b^\star$ after subtracting the along-front mean profile at the same time as in Figure 3b. Unit is m s^{-2}. (Bottom) instantaneous local energy conversions profiles HRS*, VRS* and VBF* integrated in the along-stream direction y and in the vertical. The unit of the eddy conversion terms is 10^3 J m^{-1} s^{-1}.

(10^{-12} m s^{-4} [*Deremble and Dewar*, 2012]). The mean advective PV flux, integrated vertically and longitudinally over the full Stream, increases significantly between 26°N (Figure 4e), where $\int\int q\mathbf{u} \cdot \mathrm{dS} = 0.14\,\mathrm{m}^3\,\mathrm{s}^{-4}$ and the exit of the Straits at 27°N (Figure 4g), where $\int\int q\mathbf{u} \cdot \mathrm{dS} = 0.19\,\mathrm{m}^3\,\mathrm{s}^{-4}$. The net zonal flux of PV is small, and the increase is due essentially to the frictional injection of PV at the bottom (Figure 4f), $\int\int \mathbf{J}_{\mathrm{bot}} \cdot \mathrm{dS} = 0.05\,\mathrm{m}^3\,\mathrm{s}^{-4}$.

3. Instability and Vortex Formation

The topographic interaction intensifies the positive vorticity on the cyclonic side and forms a thin filament of high vorticity, typically about 2–3 km wide (Figure 4b). Right after separation from the upper slope, the vorticity filament becomes unstable and rolls up into a string of submesoscale vortices (Figure 3).

Following the classic analysis by *Rayleigh* [1880], an isolated two-dimensional vorticity filament is always unstable and expected to roll up into discrete vortices. However, the presence of a background strain can stabilize a vorticity filament [*Dritschel et al.*, 1991]. The large-scale strain field, usually associated with coherent vortices, is an explanation for the long-time persistence of vorticity filaments in a number of laboratory and numerical experiments of two-dimensional turbulence. The strain on the cyclonic side of the Gulf Stream is large south of 27°N where the Stream is in contact with the Florida Coast and gradually decreases after leaving the Florida Straits [*Gula et al.*, 2015, Figure 18]. The vorticity of the filament after separation of the flow

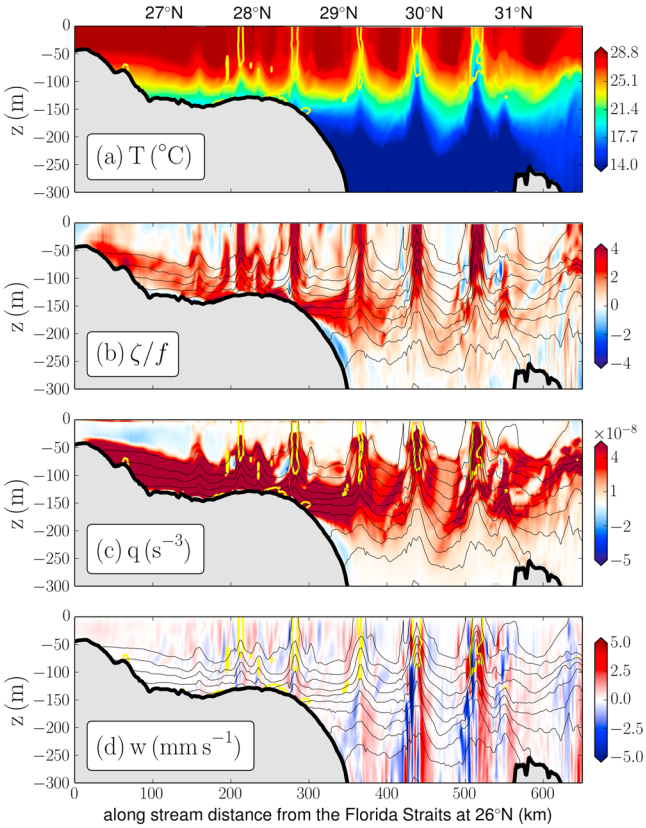

Figure 6. Temperature, relative vorticity, PV and vertical velocity at the time of Figure 3d in the along-stream direction marked as a dashed white line in Figure 3d. Black contours showing temperature and yellow contours showing relative vorticity contours are repeated on all panels.

from the coast is too large, compared to the background straining, to prevent it from becoming unstable. Unbounded flows with sufficiently strong shear layers are known to be unstable and form a vortex street [*Hide and Titman*, 1967].

We perform here a local eddy-mean analysis at the time of maximum fluctuation amplification (Figures 3b and 3f). We compute the kinetic energy conversion terms between the curved parallel flow and its meandering perturbations in a local reference frame aligned with the front following the methodology described in *Gula et al.* [2014]. The local coordinates are x and y in the cross- and along-front directions, respectively, and the corresponding horizontal velocities u and v. For this analysis the local mean, denoted by an overbar, is defined as the along-front average for the region considered. Perturbations relative to that mean are denoted with a star such that the total field of any quantity can be written $b = \overline{b} + b^\star$, $u = \overline{u} + u^\star$, $v = \overline{v} + v^\star$, and so on. An example of such a decomposition for buoyancy is shown in Figure 5 at the time and location of Figure 3b and 3f. The conversion from mean to eddy kinetic energy due to the horizontal and vertical shears are defined as stated previously, using along-front instead of time averages, $\mathrm{HRS}^\star = -\overline{\mathbf{u}^\star v^\star}\,\frac{\partial\langle\overline{\mathbf{u}}\rangle}{\partial y} - \overline{\mathbf{u}^\star u^\star}\,\frac{\partial\langle\overline{\mathbf{u}}\rangle}{\partial x}$ and $\mathrm{VRS}^\star = -\overline{\mathbf{u}^\star w^\star}\,\frac{\partial\langle\overline{\mathbf{u}}\rangle}{\partial z}$, respectively. The conversion from eddy potential to eddy kinetic energy is $\mathrm{VBF}^\star = \overline{w^\star b^\star}$, where w is the vertical velocity and b the buoyancy anomaly. The $\mathrm{HRS}^\star$ term, conversion from mean kinetic energy to eddy kinetic energy through horizontal Reynolds Stress, is the dominant term. Other sources like the vertical buoyancy flux $\mathrm{VBF}^\star$ and the vertical shear stress $\mathrm{VRS}^\star$ are smaller. The energy source for the perturbations is the horizontal shear of the mean flow. The instability is a larger-scale analogous to the horizontal shear instability of submesoscale cold filaments described in *Gula et al.* [2014].

The instantaneous barotropic energy conversion rate integrated over the volume of the Stream between 27°N and 30°N during the instability episode of Figure 5, $\int \mathrm{HRS}^\star dy = 8.1\,10^9$ J s^{-1} is about 10 times larger than the time mean barotropic energy conversion rate plotted in Figure 2 integrated over the same volume, $\int \mathrm{HRS}\, dx = 6.6\,10^8$ J s^{-1}.

The classical Charney-Stern criteria for barotropic and baroclinic instability [*Charney and Stern*, 1962], however, not formally applicable to a nonparallel flow in a non-quasi-geostrophic model, shows that necessary conditions for barotropic instability are always satisfied in the region downstream of the Straits. The cross-front PV gradient of the mean flow changes sign at the location of the vorticity maximum in the upper 50 m.

The submesoscale vortices have a diameter ≈10–15 km after formation between 27°N and 28°N. They propagate northward and grow slowly as energy from the mean flow is converted to eddy energy, and they typically reach diameters between 20 km and 30 km at 30°N. They are squeezed against the shelf in the region around 31°N, corresponding to the maximum curvature of the topography, in the sector where eddy kinetic energy is converted back to mean kinetic energy (Figure 2b).

The submesoscale vortices are surface intensified and do not extend below $z = -50$ m initially. They grow and deepen as they propagate northward. The Stream separates from the coast at 27°N at the surface (Figure 3); however, it follows the $z = -200$ m contour longer and does not separate south of 29°N (Figure 6).

Vertical along-stream sections of temperature when the flow rolls up into a string of submesoscale vortices are shown in Figure 6. Signatures of the vortices are seen in the form of negative temperature anomalies. The submesoscale vortices are associated at depth with domes of upwelled cold water, which are seen especially between 28°N and 30°N. The associated vertical velocities indicate uplift ahead of the vortices and downwelling behind associated with the thermocline dome (Figure 6). The vortices later feed into meanders at Charleston Bump that can pinch off to generate mesoscale frontal eddies [*Gula et al.*, 2015].

4. Summary and Conclusions

Meanders and eddies are routinely observed in the Gulf Stream along the South Atlantic Bight. We analyze here the instability processes that lead to the formation of submesoscale eddies on the cyclonic side of the Gulf Stream at the exit of the Straits of Florida using high-resolution realistic simulations with the Regional Oceanic Modeling System (ROMS) [*Shchepetkin and McWilliams*, 2005].

The cyclonic shear is strongly amplified as the flow moves through the Florida Straits, and the bottom boundary layer generates a narrow strip of highly positive vertical vorticity against the slope. The slope is also a strong and sustained source of positive potential vorticity that significantly contributes to the mean advective potential vorticity injected into the ocean interior.

Right after separation from the upper shelf, the thin vorticity filament becomes unstable and rolls up into a string of submesoscale vortices. The vortices grow and deepen as they propagate northward along the shelf between the exit of the Straits of Florida and the Charleston Bump. The vortices later feed into meanders at Charleston Bump, but there is not necessarily continuity between the cyclones upstream and the large slope eddies routinely observed downstream of the Charleston Bump. The details related to formation of frontal eddies through mixed barotropic-baroclinic processes at the Bump are described in *Gula et al.* [2015].

Arrested coastal waves are another mechanism by which vorticity can be created when a flow is in the direction opposite to the Kelvin wave propagation direction [*Gula and Zeitlin*, 2010; *Dewar and Hogg*, 2010]. Stratification in the boundary layer was nonetheless found to be stable, and there were no indications of flow arrest in the model.

The interactions of the tidal circulation on the shelf with the Stream, which were not included in the present study, can create another type of small-scale cyclones. *Savidge et al.* [2010] use high-frequency radars measurements to reveal sequences of short-lived cyclonic eddies along the shoreward edge of the Gulf Stream. These eddies are distinct from the submesoscale vortices described here as they are propagating equatorward and dissipate on very short time scales, typically within 1–3 h. The potential of an interaction with the processes described here will be addressed in future works by including full tidal forcings.

The process of topographic vorticity generation can be viewed as generic for boundary slope currents moving anticyclonically/cyclonically around a basin (meaning that the flow has the coast on its left/right in the Northern Hemisphere), generating strong positive/negative vorticity within the bottom boundary layer, separating over complex topography, and forming coherent submesoscale cyclonic/anticyclonic vortices. The sequence of processes described here should be also relevant for the Gulf Stream along the Florida Reef Tract, where submesoscale cyclonic frontal eddies are also frequently observed [*Kourafalou and Kang*, 2012],

and for other western boundary currents as well in the regions where they are squeezed against the continental slope.

This highlights a mechanism by which the interaction of a balanced flow with a sloping topography transfers energy from the larger-scale incident flows to submesoscale flows and provides a way toward loss of balance and energy dissipation. The submesoscale vortices will also affect vertical and cross-shelf exchanges with the adjacent shelf water, with important dynamical, ecological, and water quality implications. These processes are unaccounted for in standard oceanic models, and their impact will need to be parameterized.

Acknowledgments
We appreciate support from the Office of Naval Research (N00014-12-1-0939, N00014-12-1-0105) and the National Science Foundation (OCE-1049134). MODIS SST data are available (Level 2) at http://oceancolor.gsfc.nasa.gov/cgi/browse.pl. Model output is available upon request.

The Editor thanks two anonymous reviewers for assistance evaluating this manuscript.

References

Charney, J., and M. Stern (1962), On the stability of internal baroclinic jets in a rotating atmosphere, *J. Atmos. Sci.*, *19*, 159–172.
Deremble, B., and W. Dewar (2012), First-order scaling law for potential vorticity extraction due to wind, *J. Phys. Oceanogr.*, *42*, 1303–1313.
Dewar, W., and A. Hogg (2010), Topography inviscid dissipation of balanced flow, *Ocean Modell.*, *32*, 1–13.
Dritschel, D., P. Haynes, M. Juckes, and T. Shepherd (1991), The stability of a two-dimensional vorticity filament under uniform strain, *J. Fluid Mech.*, *230*, 647–665.
Gula, J., M. Molemaker, and J. McWilliams (2014), Submesoscale cold filaments in the Gulf Stream, *J. Phys. Oceanogr.*, *44*(10), 2617–2643.
Gula, J., M. Molemaker, and J. McWilliams (2015), Gulf Stream dynamics along the Southeastern U.S. Seaboard, *J. Phys. Oceanogr.*, *45*(3), 690–715.
Gula, J., and V. Zeitlin (2010), Instabilities of buoyancy driven coastal currents and their nonlinear evolution in the two-layer rotating shallow water model. Part I. Passive lower layer, *J. Fluid Mech.*, *659*, 69–93.
Hallberg, R., and P. Rhines (2000), Boundary sources of potential vorticity in geophysical circulations, in *IUTAM Symposium on Developments in Geophysical Turbulence*, edited by R. M. Kerr and Y. Kimura, pp. 51–65, Springer, Netherlands.
Hide, R., and C. Titman (1967), Detached shear layers in a rotating fluid, *J. Fluid Mech.*, *29*, 39–60.
Lee, T., J. Yoder, and L. Atkinson (1991), Gulf Stream frontal eddy influence on productivity of the Southeast U.S. Continental Shelf, *J. Geophys. Res.*, *96*, 22,191–22,205.
Kourafalou, V. H., and H. Kang (2012), Florida Current meandering and evolution of cyclonic eddies along the Florida Keys Reef Tract: Are they interconnected?, *J. Geophys. Res.*, *117*, C05028, doi:10.1029/2011JC007383.
Marshall, J., D. Jamous, and J. Nilsson (2001), Entry, flux, and exit of potential vorticity in ocean circulation, *J. Phys. Oceanogr.*, *31*, 777–789.
Molemaker, M., J. McWilliams, and W. Dewar (2015), Submesoscale instability and generation of mesoscale anticyclones near a separation of the California Undercurrent, *J. Phys. Oceanogr.*, *45*, 613–629.
Olson, D., O. Brown, and S. Emmerson (1983), Gulf Stream frontal statistics from Florida Straits to Cape Hatteras derived from satellite and historical data, *J. Geophys. Res.*, *88*(C8), 4569–4577.
Rayleigh, L. (1880), On the stability, or instability of certain fluid motions, *Proc. R. Soc. London*, *9*, 57–70.
Rhines, P. (1998), Circulation, convection and mixing in rotating, stratified basins with sloping topography, in *Physical Processes in Lakes and Oceans*, edited by J. Imberger, pp. 209–226, AGU, Washington, D. C.
Savidge, D., J. Norman, C. Smith, J. Amft, T. Moore, C. Edwards, and G. Voulgaris (2010), Shelf edge tide correlated eddies along the southeastern United States, *Geophys. Res. Lett.*, *37*, L22604, doi:10.1029/2010GL045236.
Shchepetkin, A., and J. McWilliams (2005), The Regional Oceanic Modeling System (ROMS): A split-explicit, free-surface, topography-following-coordinate ocean model, *Ocean Modell.*, *9*, 347–404.
von Arx, W., D. Bumpus, and W. Richardson (1955), On the fine-structure of the Gulf Stream front, *Deep Sea Res.*, *3*(1), 46–65.
Williams, R., and V. Roussenov (2003), The role of sloping sidewalls in forming potential vorticity contrasts in the ocean interior, *J. Phys. Oceanogr.*, *33*, 633–648.